International Journal of Advances in Applied Sciences (IJAAS)
Vol. 15, No. 1, March 2026, pp. 372∼383
ISSN: 2252-8814, DOI: 10.11591/ijaas.v15.i1.pp372-383

Miniaturized circular fractal patch antenna with defected ground structure for high-selectivity dual-band X-band applications

Raju Thommandru, Rengaraj Saravanakumar
Department of Electronics and Communication Engineering, Saveetha School of Engineering, Saveetha Institute of Medical and Technical Sciences, Saveetha University, Chennai, India

Article Info

Article history:

Received Sep 2, 2025
Revised Nov 17, 2025
Accepted Jan 1, 2026

Keywords:

Circular fractal patch antenna
Defected ground structure
Dual-band operation
Miniaturization
X-band

ABSTRACT

Microstrip patch antennas are easily fabricated and have a low profile, making them widely used in radar, satellite, and defence applications. Achieving high selectivity and miniaturization in X-band dual-band operation remains a challenge. Conventional designs using simple patch geometries and defected ground structures (DGS) often exhibit limited bandwidth, poor impedance matching, and reduced gain. To address these limitations, this work presents a miniaturized circular fractal patch antenna with an optimized DGS to enhance frequency selectivity, improve impedance matching, and maintain compact size. Circular fractal slots are introduced in the radiating patch to extend the effective current path while preserving the footprint. A centrally placed diamond-shaped slot provides capacitive loading that aids impedance tuning. Electromagnetic simulations were conducted in Ansys HFSS 2023 R2, and a prototype was fabricated on an FR-4 substrate with $\varepsilon_r = 4.4$, loss tangent $= 0.02$, and thickness $1.6\,\mathrm{mm}$. Measurements verify two passbands: 8.637–$9.173\,\mathrm{GHz}$ (center $8.8025\,\mathrm{GHz}$, return loss $-22.0267\,\mathrm{dB}$, voltage standing wave ratio (VSWR) 1.1720, gain $4.82\,\mathrm{dB}$, efficiency 63.51%) and 10.121–$10.956\,\mathrm{GHz}$ (center $10.3700\,\mathrm{GHz}$, return loss $-25.2864\,\mathrm{dB}$, VSWR 1.1199, gain $3.42\,\mathrm{dB}$, efficiency 72.58%). The antenna shows steady radiation and improved matching across both bands, supporting use in compact X-band front ends.

Corresponding Author:

Rengaraj Saravanakumar
Department of Electronics and Communication Engineering, Saveetha School of Engineering
Saveetha Institute of Medical and Technical Sciences, Saveetha University
Chennai, India
Email: saravanakumarr.sse@saveetha.com

1. INTRODUCTION

Microstrip patch antennas have emerged as one of the key components in contemporary wireless technologies because of their low profile, light weight, and easy-to-integrate features with radio frequency (RF) front ends. This class of antennas supports use in satellite links, weather monitoring, remote sensing, radar, and defense. The X-band ($8\,\mathrm{GHz}$ to $12\,\mathrm{GHz}$) is particularly important for surveillance radars, space missions, and military communications, where compact, efficient, and multi-functional radiators are essential.

Despite these advantages, microstrip patches face constraints that include narrow impedance bandwidth, moderate gain, and reduced efficiency under miniaturization. Achieving a compact dual-band response in the X-band is difficult because size reduction, impedance matching, radiation efficiency, and

selectivity often pull in different directions. Bandwidth enhancement is commonly pursued through parasitic elements, multiple resonators, or defected ground structures (DGS), but these methods may enlarge the footprint, introduce unwanted modes, or disturb pattern stability. Fractal geometries such as Sierpinski, Koch, and Minkowski can lengthen the current path for multiband behavior and smaller size. However, many fractal designs target lower frequency services (for example, GSM and WLAN), and reported X-band implementations frequently show limited efficiency or insufficient frequency selectivity.

Recent studies have investigated hybrid strategies that integrate fractal geometries with ground modifications or slotting to achieve dual-band or multiband functionality. For example, Koch and Minkowski fractal patches coupled with DGS have shown improved impedance bandwidth and reduced size, but often at the cost of complex geometries and fabrication challenges. Other works relying solely on DGS-based enhancements tend to improve impedance characteristics but lack sufficient frequency selectivity or compactness for X-band applications. These gaps motivate the need for a design that combines miniaturization, efficiency, and high selectivity within a single, compact architecture.

To overcome these limitations, a miniaturised circular fractal patch antenna with an integrated DGS for dual-band X-band operation has been proposed in this work. The proposed antenna uses circular fractal slotting to lengthen the effective current path length and introduce multiple resonances, the central diamond-shaped slot to realize capacitive loading to improve impedance matching, and optimized rectangular DGS with symmetric notches to suppress surface waves and improve the frequency selectivity of the antenna. The novelty of this design is the synergistic combination of fractal slotting and DGS to achieve dual-band operation with deep return loss notches, stable broadside radiation and high radiation efficiency in an ultra-compact footprint.

The contributions of this work are threefold:

- Development of a compact circular fractal antenna geometry optimized for dual-band X-band performance.
- Integration of a mid-diamond slot and DGS to simultaneously enhance impedance matching, radiation efficiency, and selectivity.
- Experimental validation of the proposed antenna, demonstrating dual resonances in the X-band with superior return loss, voltage standing wave ratio (VSWR), gain, and efficiency compared to conventional fractal or DGS-only counterparts.

Several recent works have explored dual-band and fractal antenna designs relevant to X-band applications. Rajpoot *et al.* [1] presented an aperture-coupled diagonal square fractal antenna with a low profile operating at 5.9 GHz and 9.5 GHz, delivering gains of 2.43 dBi and 7.88 dBi. The design attains good efficiency but occupies a comparatively larger footprint, and the notable gain increase appears mainly in the higher band. Pande *et al.* [2] introduced a dual-band metasurface patch with varactor and PIN-diode tuning at 2.6 GHz and 3.4 GHz, achieving a gain of 7.5 dBi; these operating bands are below the X-band.

Cheng *et al.* [3] presented a dual-band shared-aperture antenna spanning 2.09–11.61 GHz and 21.6–29.6 GHz. Although the first range includes the X-band, the wide coverage constrains targeted dual-band optimization. Kumar *et al.* [4] designed a flexible coplanar waveguide (CPW)-fed antenna for 10.5–12 GHz with 6 dBi gain, focusing on circular polarization rather than compact dual-band performance. Mianji *et al.* [5] reported a fractal triangular microstrip antenna at 3.0 GHz and 5.8 GHz with excellent return loss, but outside X-band. Jenath *et al.* [6] presented multi-band hybrid fractal antenna covering 2.12–2.95 GHz and 4.82–5.95 GHz, lacking X-band operation. Attioui *et al.* [7] presented a Sierpinski carpet fractal antenna at 4.88, 9.62, and 10.03 GHz, close to the desired X-band range though with weaker matching in first band. Marzouk *et al.* [8] developed a printed multiband fractal triangular antenna (1.84–5.79 GHz), not targeting X-band.

Lavanya and Kumari [9] designed a dual-band fractal patch with reactive impedance surface (RIS) and Mushroom unit cell (MUC) at 2.4 GHz and 3.35–3.71 GHz, unsuitable for X-band. Al-Rawe *et al.* [10] presented a dual band fractal rectenna for energy harvesting at 2.45 GHz and 5.8 GHz, which does not target the X-band. Bui *et al.* [11] reported a dual band, dual polarised slotted patch operating at 2.45 GHz and 5.25 GHz. Sood and Rai [12] reported a compact fractal patch covering 8.62 GHz to 22.4 GHz; however, the achieved gain is lower than typical X–band designs. Srikanta and Pachiyaannan [13] introduced a dual-band fractal antenna through truncated hexagonal rings (4.6–6.7 GHz, 12–14.2 GHz, missing desired X-band points). Shankar and Upadhyay [14] proposed a fractal monopole antenna (7.95–12.64 GHz) with dual polarization, covering X-band but without return loss data. Kumar *et al.* [4] designed a flexible CPW antenna for X-band (10.5–12 GHz) with 6 dBi gain and AR $<$ 3 dB on a compact 27$\times$28 mm polyimide substrate, ideal for conformal uses. However, the operational band is narrow compared to wideband needs.

Rajavel and Ghoshal [15] proposed a compact multiband reconfigurable antenna with artificial magnetic conductor (AMC), covering 8.7, 10.5, and 11.4 GHz, achieving 3.29 dB gain enhancement, 87% efficiency, and SAR as low as 0.0594 W/kg. The larger size and PIN diode biasing network are drawbacks. Singh *et al.* [16] developed an artificial neural network (ANN)-based O-shaped slotted microstrip patch antenna with –26.44 dB return loss at 1.68 GHz and accurate bandwidth prediction (1.308% error), but it targets L-band rather than X-band. Yaminisasi *et al.* [17] reported a fish-tail fractal monopole with defected partial ground structure (DPGS) that operates over 2.5–4.2 GHz and 7–9.8 GHz with gains approaching 5 dBi. The design is compact, yet it does not align precisely with the targeted X-band centers at 8.8025 GHz and 10.3700 GHz. Elsalam *et al.* [18] introduced a low specific absorption rate (SAR) semicircular slot antenna with DGS covering 1.8–3.7 GHz and 4.05–5.5 GHz and achieving a peak gain of 8.5 dBi; its focus is 5G rather than X-band. Mohini and Saravanakumar [19] presented a wearable high-gain DGS antenna tailored to 6 GHz body-area links, which remains under X-band. Dharani *et al.* [20] report that moving from a full ground to a restricted ground in a multiband patch improves matching and bandwidth by altering the current paths beneath the radiator. Chakraborty *et al.* [21] apply similar ground engineering in a compact unified S-band monopole multi-input multi-output (MIMO) to raise isolation but the gain can come with efficiency loss and sensitivity to device ground and user proximity. Xu and Wang [22] reduce coupling in dual-band WLAN MIMO using a WM-shaped DGS which achieves isolation improvement through slot design that operates as a frequency-selective current filter at different bands.

The structure of the work is detailed as follows. Section 2 presents the antenna geometry and the design workflow. Section 3 provides simulation and measurement results. Section 4 distills design insights and salient observations. Section 5 concludes with application contexts and brief directions for future investigation.

2. SYSTEM METHODOLOGY

This work develops a compact circular fractal patch antenna with a DGS for dual-band operation within the X-band. The methodology covers three stages: i) geometric formulation of the radiating element and ground plane, ii) full-wave electromagnetic modeling, and iii) simulation-driven assessment of impedance and radiation characteristics. The patch employs circular fractal slotting to lengthen the surface current path, while a centrally placed diamond-shaped aperture introduces capacitive loading that assists impedance matching. The ground plane incorporates a DGS to suppress surface waves and to widen the usable bandwidth. The overall configuration appears in Figure 1; the circular fractal patch is highlighted in Figure 1(a) and the corresponding ground topology in Figure 1(b).

(a) (b)

Figure 1. Proposed antenna configuration: (a) circular fractal patch with a mid-diamond slot that increases the effective current path and aids matching and (b) DGS that mitigates surface waves and enlarges bandwidth

Figure 2 summarizes the design evolution of the ground plane that is used to tune input impedance and radiation behavior. Panels illustrate the proposed ground, a full ground, a half ground, and a ring–type DGS. A fully metallized ground serves as the reference and exhibits limited frequency selectivity with stronger surface-wave content. Reducing the ground to a partial layout improves matching, but it can raise inter-modal coupling. Introducing a ring-type DGS adds periodic stopbands and perturbs ground currents, which lowers surface-wave energy and enhances isolation. The final design combines a partial ground clearance with patterned DGS apertures so that the return path is shaped and the effective electrical length increases. This

sequence from simple to patterned grounds steers the current distribution, enables robust dual-band excitation, and maintains a stable main lobe without excessive intrusion into the ground region.

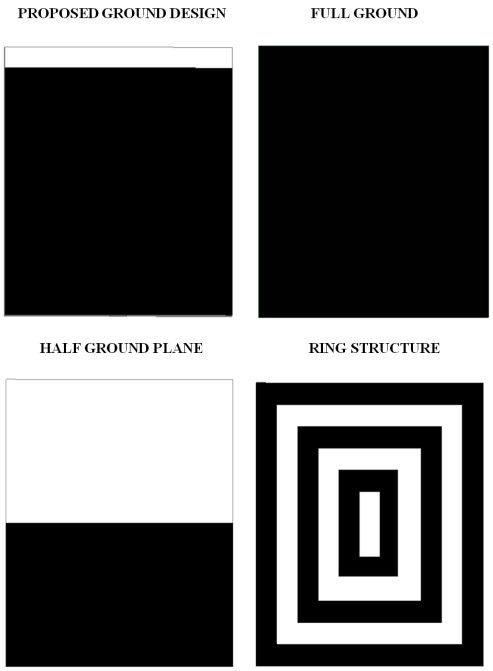

Figure 2. Design evolution of the ground plane

2.1. Antenna geometry and design principle

The radiating patch in Figure 1(a) adopts a circular fractal layout that lengthens the effective current path while preserving the footprint, which facilitates multiple resonances within the X-band. A centrally placed diamond-shaped slot provides capacitive loading that improves input matching and allows fine control of the resonant frequencies. The defected ground in Figure 1(b) consists of a rectangular aperture of $12\ \mathrm{mm} \times 8\ \mathrm{mm}$ with two symmetric notches of $4\ \mathrm{mm} \times 3\ \mathrm{mm}$. This pattern perturbs the ground currents, reduces surface-wave content, and broadens the impedance bandwidth. The antenna is realized on a substrate of $26\ \mathrm{mm} \times 22\ \mathrm{mm}$ with thickness $1.6\ \mathrm{mm}$. The circular patch has an effective radius of $7.5\ \mathrm{mm}$, fed by a $3\ \mathrm{mm}$ wide and $10\ \mathrm{mm}$ long microstrip line for 50 Ω matching. These optimized dimensions ensure compactness while maintaining stable dual-band resonance. The antenna is realized on an FR-4 substrate with relative permittivity $\varepsilon_r = 4.4$ and loss tangent 0.02. The fundamental resonance of the circular patch is estimated using (1). Optimized geometric parameters are summarized in Table 1 to support reproducibility and design transparency.

$$f_r = \frac{1.8412 \cdot c}{2\pi a_e \sqrt{\varepsilon_r}} \tag{1}$$

Table 1. Optimized dimensions of the proposed antenna

Parameter	Value (mm)
Substrate length (L_{sub})	26
Substrate width (W_{sub})	22
Patch radius (a_p)	7.5
Diagonal of mid-diamond slot	3.0
Ground-plane slot length (L_g)	12
Ground-plane slot width (W_g)	8
Feed notch length (L_n)	4
Feed notch width (W_n)	3
Microstrip width (W_f)	3.0
Microstrip length (L_f)	10
Substrate thickness (h)	1.6

2.2. Defected ground structure integration

After fixing the circular patch geometry, a DGS is etched beneath the radiator to control guided currents on the ground plane. The perturbation weakens surface-wave channels, which reduces dielectric loss and increases the usable impedance bandwidth. The modified current paths also raise radiation efficiency and help limit back-lobe levels. The slot pattern reshapes the return path and introduces an equivalent inductance L and capacitance C set by the slot length, gap spacing, and coupling to the patch. The DGS therefore acts as a resonant cell with a band-stop response. Its cut-off frequency is (2).

$$f_c = \frac{1}{2\pi\sqrt{LC}} \tag{2}$$

Where L and C summarize the electromagnetic storage produced by the defect geometry. By selecting the slot dimensions to target the undesired spectral region, the band-stop action suppresses parasitic harmonics and improves isolation between the dual resonant bands.

2.3. Impedance matching and return loss

With the DGS in place, the input impedance Z_{in} is tuned toward the $50\ \Omega$ feed. Any departure from $Z_0 = 50\ \Omega$ produces a reflected component quantified by the voltage reflection coefficient (3).

$$\Gamma = \frac{Z_{\text{in}} - Z_0}{Z_{\text{in}} + Z_0} \tag{3}$$

The return loss in decibels follows from the magnitude of Γ (4).

$$RL\ (\text{dB}) = -20\log_{10}|\Gamma| \tag{4}$$

Two geometric levers are used to meet the match. First, circular fractal slotting increases the effective current path, which shifts the resonant poles and balances the resistive and reactive parts of Z_{in}. Second, the mid-diamond aperture adds capacitive loading that offsets the inductive content introduced by the fractalization. The DGS provides a third lever by altering ground-plane currents, which enables fine control of the input reactance. Together these elements yield stable multi-resonant behavior across the targeted X-band subranges with low $|\Gamma|$ and improved RL.

2.4. Radiation efficiency

Radiation efficiency η_{rad} quantifies the fraction of the input power that emerges as radiated power. It is defined as (5).

$$\eta_{\text{rad}} = \frac{P_{\text{rad}}}{P_{\text{in}}} \tag{5}$$

With P_{rad} the radiated power and P_{in} the accepted input power. In printed antennas the dominant loss channels arise from finite conductor conductivity, dielectric loss tangent, and energy bound to surface waves. The present layout mitigates these channels by two mechanisms. First, the circular fractal slot redistributes surface currents and lowers current crowding near feed transitions, which reduces ohmic loss. Second, the DGS weakens surface-wave propagation so that a larger share of the stored energy couples into space waves rather than being guided within the substrate. Together these effects raise η_{rad} across the operating band.

2.5. Gain and directivity

Antenna gain combines directivity and efficiency. It is written as (6).

$$G = \eta_{\text{rad}} \cdot D \tag{6}$$

Where D denotes the directivity that follows from the angular power distribution independent of loss. In the proposed patch, the circular fractal motif guides the current toward a balanced aperture field, which improves D and limits pattern distortion. The mid-diamond slot contributes capacitive loading that refines the phase of the aperture field. The DGS complements these actions by reducing power leakage into the substrate and by trimming back radiation, so the realized gain improves without sacrificing beam stability.

2.6. Simulation and evaluation

The design was evaluated in Ansys HFSS 2023 R2. Simulations extracted S_{11}, VSWR, gain, radiation efficiency, impedance bandwidth, and far-field patterns. The workflow used adaptive meshing with convergence on the complex input impedance to ensure mesh independence of the reported figures. The simulated resonant frequencies were compared with the analytical estimate in (1), and the DGS notch behavior was assessed against the cut-off prediction in (2). The two checks were consistent within the expected limits set by substrate dispersion and fringe fields, which indicates that the equivalent models capture the governing physics of the radiator and ground. The resulting dataset provides a reproducible reference for subsequent fabrication and for studies that seek to retune the dual-band response by modifying the slot geometry or the DGS cell dimensions.

3. RESULTS

This section reports the measured performance of the antenna within the X-band. The discussion links input impedance metrics to far-field behavior and efficiency. These parameters are used to assess suitability for selective dual-band operation.

3.1. Return loss analysis

Figure 3 shows the measured input reflection coefficient from 8 GHz to 12 GHz. A dual-band response is obtained. The first operating band extends from 8.637 GHz to 9.173 GHz, with a resonance at 8.8025 GHz where the return loss reaches -22.0267 dB. This level is well under the -10 dB criterion and indicates a strong impedance match. The second operating band covers 10.121 GHz to 10.956 GHz, with a resonance at 10.3700 GHz and a return loss of -25.2864 dB. The two deep notches reflect high frequency selectivity, while the fractional bandwidths of each band support multi-channel operation. The circular fractal slotting and the DGS contribute to these results by enlarging the effective current path and suppressing surface waves, which improves the impedance locus around both resonances.

The comparison in Figure 4 indicates good alignment between simulation and measurement. Minor shifts in the notch frequencies are consistent with fabrication tolerances, substrate parameter spread, and connector parasitics. The preservation of both resonances confirms that the modeled mechanisms governing the dual-band response are realized in hardware.

3.2. VSWR analysis

The VSWR was measured over same 8 to 12 GHz range and is shown in Figure 5. The first resonance at 8.8025 GHz yields a VSWR of 1.1720, which corresponds to $S_{11} = -22.0267$ dB. The second resonance near 10.3750 GHz records a VSWR of 1.1199, consistent with $S_{11} = -25.2864$ dB. Across 8.637–9.173 GHz and 10.121–10.956 GHz the VSWR remains under 2, indicating robust impedance matching throughout both passbands. The close correspondence between the VSWR minima and the return loss notches validates the matching strategy that combines fractal slotting on the patch with a patterned ground.

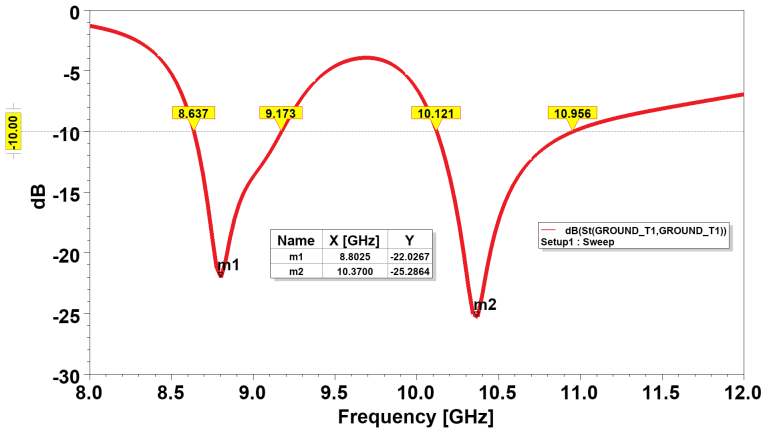

Figure 3. Measured S_{11} with resonances at 8.8025 GHz (-22.0267 dB) and 10.3700 GHz (-25.2864 dB)

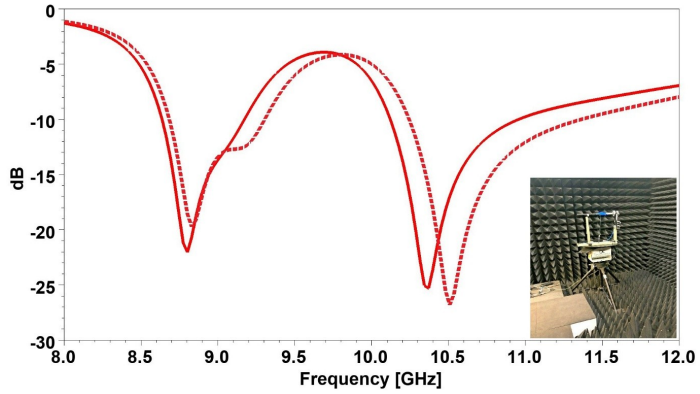

Figure 4. Simulated and measured S_{11} showing close agreement at 8.8025 GHz and 10.3700 GHz

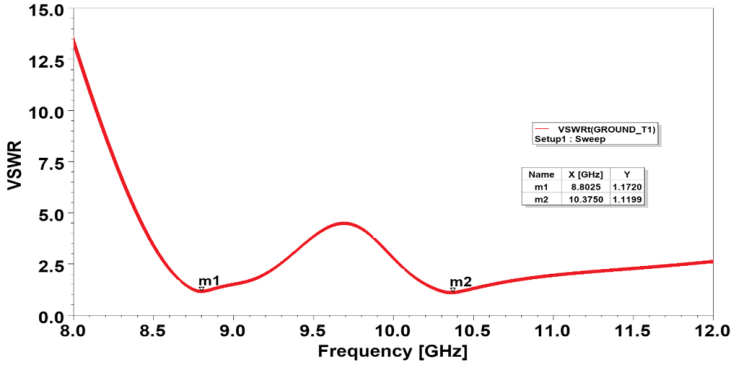

Figure 5. Measured VSWR across 8–12 GHz with minima of 1.1720 at 8.8025 GHz and 1.1199 at 10.3750 GHz

3.3. Gain and directivity analysis for plot 1

The three-dimensional radiation behavior at 8.8025 GHz is summarized in Figure 6. From Figure 6(a), the realized peak gain is 4.81698 dB, which indicates efficient conversion of accepted power into radiation in the preferred look direction. From Figure 6(b), the corresponding directivity is 6.22480 dB, which reflects a concentrated main beam. The difference between directivity and gain follows from conductor and dielectric losses in the FR4 substrate with loss tangent 0.02. The three-dimensional patterns exhibit a clean broadside main lobe with low sidelobe levels, so the transmitted power is largely confined to the intended coverage sector.

3.4. Gain and directivity analysis for plot 2

Figure 7 reports the radiation characteristics at the second resonance of 10.3700 GHz. The peak gain equals is 3.41829 dB as shown in Figure 7(a), referenced to an isotropic radiator. The peak directivity is 5.39011 dB as shown in Figure 7(b), which confirms a focused broadside beam. The gap between directivity and gain is consistent with residual ohmic and dielectric loss. The radiation surfaces show smooth beam contours with low sidelobes, which supports short to medium range X-band links where pattern stability and limited interference are required.

3.5. Two-dimensional gain and directivity trends

Figure 8 presents the frequency evolution of gain and directivity over 8–12 GHz. At 8.8025 GHz, the measured peak gain is 4.81698 dB and the directivity is 6.22480 dB. The gap is about 1.41 dB and follows from conductor and dielectric loss. At 10.3700 GHz, the gain is 3.41829 dB and the directivity is 5.39011 dB, giving a gap of about 1.97 dB. Across the scanned band the curves are smooth, with directivity above 5 dB near both resonances and gain above 3 dB, which satisfies the selectivity requirements for the intended X-band operation.

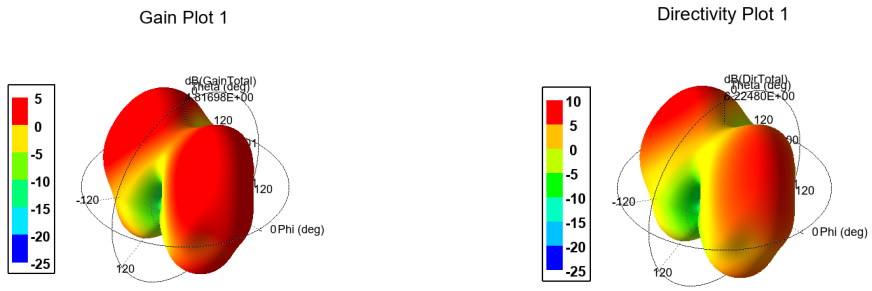

(a) (b)

Figure 6. Three-dimensional patterns at 8.8025 GHz: (a) gain $= 4.81698$ dB and (b) directivity $= 6.22480$ dB

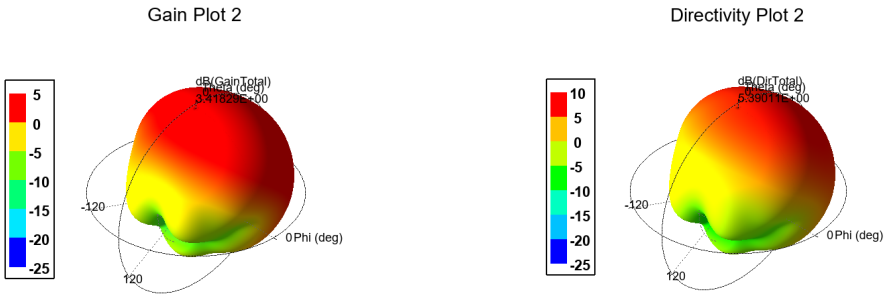

(a) (b)

Figure 7. Three-dimensional patterns at 10.3700 GHz: (a) peak gain $= 3.41829$ dB and (b) peak directivity $= 5.39011$ dB

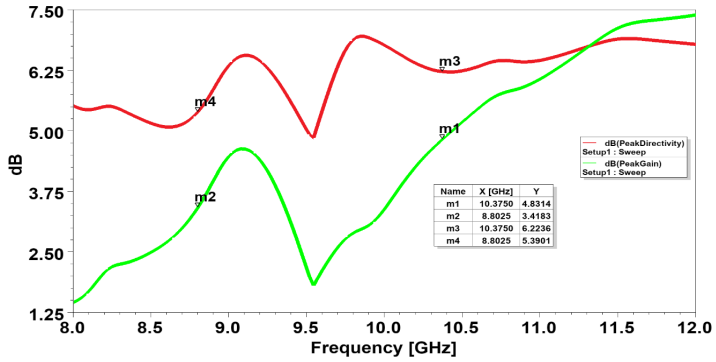

Figure 8. Two-dimensional gain and directivity across 8–12 GHz

3.6. Radiation efficiency analysis

The antenna radiation efficiency over the 8–12 GHz is shown in Figure 9. It shows stable performance in both working bands. At the first resonance of 8.8025 GHz, the measured efficiency is 63.51%, indicating that nearly two-thirds of the input power is converted into radiated energy, with the remainder lost mainly due to dielectric losses in the FR4 substrate ($\tan\delta = 0.02$) and minor conductor losses in the feed and patch metallization. At the second resonance of 10.3750 GHz, efficiency improves to 72.58%, reflecting reduced surface wave losses and a more favorable current distribution, which also explains the corresponding gain increase in this band. Across the measured spectrum, efficiency remains above 40%, even outside the

resonances, confirming that the antenna maintains functional radiation capability over a wide span. These results show that the design is always efficient in both bands with resonant points, a fact that matches the operational requirements of highly selective X-band application.

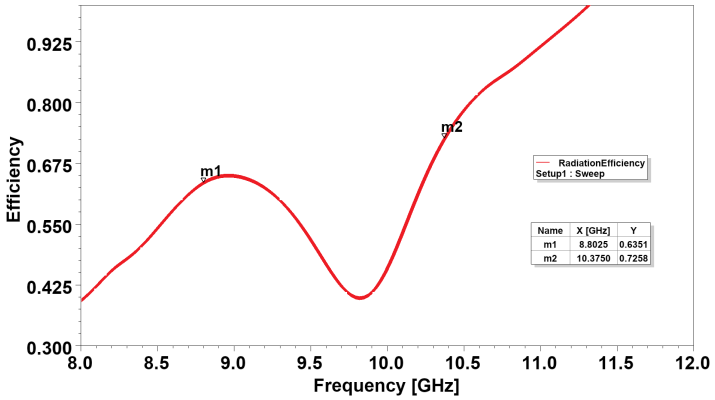

Figure 9. Measured radiation efficiency with 63.51% at 8.8025 GHz and 72.58% at 10.3750 GHz

3.7. Fabricated prototype and measurement setup

The fabricated antenna is shown in Figure 10. A board on FR-4 was etched using standard PCB steps, an SMA was soldered to the microstrip feed, and measurements were taken on a vector network analyzer. Figure 10(a) details the top metallization with the circular fractal radiator and mid-diamond slot, while Figure 10(b) depicts the defected ground on the reverse side. The measured S_{11} follows the simulated curve across the band, supporting the selected geometry.

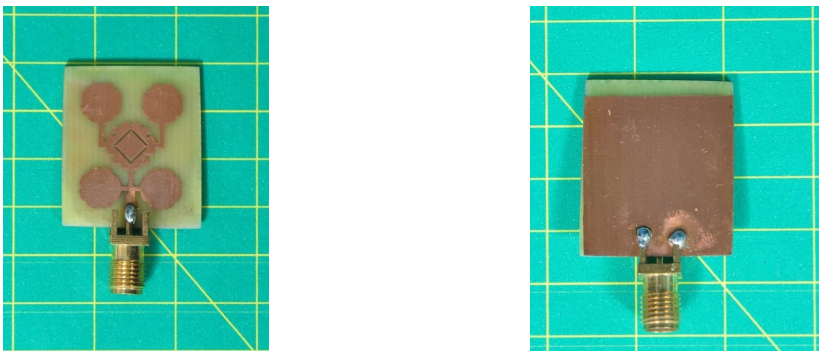

(a) (b)

Figure 10. Fabricated antenna prototype: (a) top view with circular fractal patch and mid-diamond slot and (b) bottom view with DGS

4. DISCUSSION

The proposed miniaturized circular fractal patch antenna with DGS was experimentally evaluated across the 8–12 GHz X-band to establish its suitability for compact high-selectivity dual-band operation. Measured return loss (S_{11}) revealed two distinct resonances: 8.637–9.173 GHz (centered at 8.8025 GHz, –22.0267 dB) and 10.121–10.956 GHz (centered at 10.3700 GHz, –25.2864 dB), both exceeding the standard –10 dB impedance-matching criterion. The combined action of the circular fractal slotting, which lengthens the current path, and the optimized DGS, which suppresses surface waves and evens the ground return, produces deep return-loss notches and stable dual-band behavior. VSWR remains under 2 in both passbands, with minima of 1.1720 at 8.8025 GHz and 1.1199 at 10.3750 GHz, which confirms effective impedance control. Radiation analysis yields a peak gain of 4.82 dB with directivity of 6.22 dB at 8.8025 GHz, and 3.42 dB

gain with 5.39 dB directivity at 10.3700 GHz. The gap between directivity and gain follows from dielectric and conductor losses in FR4 with loss tangent 0.02. Three-dimensional patterns at both resonances show a dominant broadside main lobe and low sidelobes, which maintains beam stability and concentrates radiated power. Using standard FR4 of thickness 1.6 mm and $\varepsilon_r = 4.4$ supports low-cost PCB fabrication and straightforward integration with RF front ends and arrays. Measured radiation efficiency is 63.51% at 8.8025 GHz and 72.58% at 10.3750 GHz. Outside the resonant peaks the efficiency stays above 40%. The compact footprint of $22 \text{ mm} \times 26 \text{ mm}$ suits embedded X-band radar modules, satellite terminals, and portable defense radios.

A brief comparison with recent fractal and DGS designs highlights the distinct operating regime of the present antenna. The Sierpinski carpet fractal with DGS in [23] targets 2.45 and 5.8 GHz for industrial, scientific, and medical (ISM) use. The Koch fractal with DGS in [24] covers 1.9–4.3 GHz with 4 dBi gain and 77% bandwidth. A low-profile wearable DGS antenna in [19] is optimized near 6 GHz. The Koch–hexagonal combined circular radiator in [25] spans 2.38–5.80 GHz, and the fish-tail fractal monopole in [17] provides dual broadband around 3.22, 7.64, and 9.41 GHz. In contrast, the proposed layout operates in the X-band with resonances at 8.8025 and 10.3700 GHz, exhibits deep return loss of -22.0267 and -25.2864 dB, delivers competitive gains of 4.82 and 3.42 dB, and retains a compact $22 \text{ mm} \times 26 \text{ mm}$ form factor. As summarized in Table 2, this combination of selectivity, efficiency, and size positions the design for high-frequency radar and satellite links that require miniaturization without complex fabrication.

Although the prototype meets the target specifications, the FR4 substrate introduces dielectric loss that slightly lowers realized gain and radiation efficiency relative to low-loss laminates. The geometry is tuned to two X-band sub-bands, so broader multiband coverage would require systematic scaling and substrate refinement. Future work will examine low-loss materials to raise efficiency, reconfigurable loading for tunable operation, and array-level integration to enable beam steering. Environmental testing over temperature and humidity ranges will also be conducted to quantify long-term stability and to confirm readiness for field deployment.

Table 2. Optimized dimensions of the proposed antenna

Author (year)	Operating bands (GHz)	Size (mm)	Gain (dBi)	Efficiency (%)
Sierpinski carpet fractal + DGS [23]	2.45 / 5.8	40×40	3.2–5.1	70
Koch fractal antenna + DGS [24]	1.9–4.3	38×34	4.0	77
Fish-tail fractal monopole [17]	3.22 / 7.64 / 9.41	30×28	5.0	68
Flexible CPW-fed [15]	10.5–12	27×28	6.0	–
Proposed work	8.64–9.17 / 10.12–10.96	22×26	4.82 / 3.42	63.5 / 72.6

5. CONCLUSION

This research presented a compact circular fractal patch antenna with a DGS for selective dual-band operation in the X-band. The geometry combines a circular fractal motif with a mid-diamond slot to lengthen the current path and to improve input matching within a $22 \text{ mm} \times 26 \text{ mm}$ footprint. Measurements verify two resonances. At 8.8025 GHz the antenna achieves $S_{11} = -22.0267$ dB, VSWR $= 1.1720$, gain $= 4.82$ dB, and radiation efficiency $= 63.51\%$. At 10.3700 GHz the results are $S_{11} = -25.2864$ dB, VSWR $= 1.1199$, gain $= 3.42$ dB, and radiation efficiency $= 72.58\%$. Both passbands, 8.637–9.173 GHz and 10.121–10.956 GHz, exhibit broadside patterns with low sidelobes and smooth gain–directivity behavior. The data indicate strong impedance control, high efficiency for an FR4 substrate, and effective miniaturization. In view of the measured performance and size, the design is well suited to X-band radar front ends, satellite links, and compact defense transceivers that require stable matching and controlled radiation within constrained form factors.

FUNDING INFORMATION

No funding was received for this work.

AUTHOR CONTRIBUTIONS STATEMENT

This journal uses the Contributor Roles Taxonomy (CRediT) to recognize individual author contributions, reduce authorship disputes, and facilitate collaboration.

Name of Author	C	M	So	Va	Fo	I	R	D	O	E	Vi	Su	P	Fu
Raju Thommandru	✓	✓	✓	✓	✓	✓		✓	✓	✓			✓	
Rengaraj Saravanakumar		✓				✓		✓	✓	✓	✓	✓		

C : **C**onceptualization
M : **M**ethodology
So : **So**ftware
Va : **Va**lidation
Fo : **Fo**rmal Analysis
I : **I**nvestigation
R : **R**esources
D : **D**ata Curation
O : Writing - **O**riginal Draft
E : Writing - Review & **E**diting
Vi : **Vi**sualization
Su : **Su**pervision
P : **P**roject Administration
Fu : **Fu**nding Acquisition

CONFLICT OF INTEREST STATEMENT

Authors state no conflict of interest.

DATA AVAILABILITY

Derived data supporting the findings of this study are available from the corresponding author, [RS], on request.

REFERENCES

[1] S. Rajpoot, S. Ghosh, and M. V. Swati, "A low-profile, aperture-coupled, diagonal square fractal antenna for dual-band vehicular communication," *International Journal of Communication Systems*, vol. 38, no. 4, 2025, doi: 10.1002/dac.70003.

[2] S. Pande, D. Patil, A. Kumar, A. Tyavlovsky, and A. Muthanna, "Design of a metasurface loaded with RF varactor and PIN diode integration dual-band reconfigurable antenna for bluetooth, Wi-Fi, WLAN and wireless 5G applications," *Physica Scripta*, vol. 100, no. 2, Feb. 2025, doi: 10.1088/1402-4896/adac15.

[3] J. Cheng, T. Gao, D. Han, and C. Zhou, "Dual-band shared-aperture antenna with pattern and polarization diversity," *Applied Sciences*, vol. 15, no. 2, Jan. 2025, doi: 10.3390/app15020878.

[4] D. R. Kumar, K. Vishnulakshmi, K. G. S. Narayan, and G. V. Babu, "Flexible circularly polarized CPW antenna for X-band: design, simulation, and experimental validation," *Engineering Research Express*, vol. 7, no. 1, pp. 1-12, Feb. 2025, doi: 10.1088/2631-8695/adaada.

[5] A. Mianji, M. Bemani, S. Nikmehr, and A. A. Gargari, "Design of dual-band triangular microstrip antenna using fractal structure for wi-max and wi-fi applications," in *2024 32nd International Conference on Electrical Engineering*, May 2024, pp. 1–5, doi: 10.1109/ICEE63041.2024.10667946.

[6] M. Jenath, R. Prasanna, P. B. Priya, and S. Hariganesan, "Design of multi-band hybrid fractal antenna for wireless application," in *2024 International Conference on Communication, Computing and Internet of Things*, Apr. 2024, pp. 1–4, doi: 10.1109/IC3IoT60841.2024.10550341.

[7] S. Attioui, A. Khabba, S. Ibnyaich, and A. Zeroual, "Design of a dual band antenna for wireless communications utilizing the sierpinski carpet fractal," *ITM Web of Conferences*, vol. 69, Dec. 2024, doi: 10.1051/itmconf/20246904001.

[8] M. Marzouk, Y. Rhazi, I. H. Nejdi, and M. Saih, "A new printed multiband fractal triangular antenna for wireless application," *TELKOMNIKA (Telecommunication Computing Electronics and Control)*, vol. 22, no. 1, pp. 55-64, Oct. 2023, doi: 10.12928/telkomnika.v22i1.25006.

[9] V. Lavanya and U. R. Kumari, "Compact dual band fractal patch antenna based on RIS and MUC," *Research Square*, 2023, doi: 10.21203/rs.3.rs-2650329/v1.

[10] T. S. A. Al-Rawe, T. A. Elwi, and Ö. Ü. D. K. Türeli, "A dual-band high efficiency fractal rectenna for RF energy harvesting systems," in *2023 5th International Congress on Human-Computer Interaction, Optimization and Robotic Applications*, Jun. 2023, pp. 1–4, doi: 10.1109/HORA58378.2023.10156661.

[11] T. H. Bui, H. T. Vu, S. X. Ta, K. K. Nguyen, C. D.- Ngoc, and N. N.- Trong, "Dual-band dual-polarized slotted-patch antenna for in-band full-duplex applications," *IEEE Antennas and Wireless Propagation Letters*, vol. 22, no. 6, pp. 1286–1290, Jun. 2023, doi: 10.1109/LAWP.2023.3240831.

[12] M. Sood and A. Rai, "Design of compact fractal patch antenna for X/Ku/K-band applications," *International Journal of Communication Systems*, vol. 36, no. 11, Jul. 2023, doi: 10.1002/dac.5515.

[13] N. Srikanta and M. Pachiyaannan, "A dual band fractal antenna with truncated hexagonal nested rings for wireless applications," in *2023 7th International Conference on Trends in Electronics and Informatics*, Apr. 2023, pp. 67–71, doi: 10.1109/ICOEI56765.2023.10125628.

[14] S. Shankar and D. K. Upadhyay, "A fractal monopole antenna with dual polarization reconfigurable characteristics for X-band applications," *IEEE Access*, vol. 11, pp. 95667–95680, 2023, doi: 10.1109/ACCESS.2023.3311133.

[15] V. Rajavel and D. Ghoshal, "A compact multiband frequency reconfigurable antenna integrated with sextuple band artificial magnetic conductor for heterogeneous wireless applications," *Frequenz*, vol. 79, no. 3–4, pp. 143–166, Apr. 2025, doi: 10.1515/freq-2024-0193.

[16] O. Singh, S. K. Sriwas, and S. Ayub, "ANN-based design analysis of O-shaped slotted microstrip patch antenna for L band applications," *International Journal of Electronics*, vol. 112, no. 10, pp. 2311–2326, Oct. 2025, doi: 10.1080/00207217.2025.2450731.

[17] G. Yaminisasi *et al.*, "Fish-tail structured fractal monopole printed antenna with dual broadband characteristics for Sub–6GHz 5G and X–band radar applications," *Fractal and Fractional*, vol. 9, no. 1, Jan. 2025, doi: 10.3390/fractalfract9010029.
[18] R. W. A.- Elsalam, H. E. Seleem, M. M. A.- Elnaby, and A. H. Hussein, "Low SAR compact wideband/dual-band semicircular slot antenna structures for sub-6 GHz 5G wireless applications," *EURASIP Journal on Wireless Communications and Networking*, vol. 2025, no. 1, Jan. 2025, doi: 10.1186/s13638-024-02424-x.
[19] T. Mohini and R. Saravanakumar, "High-gain, low-profile defected ground antenna for wearable medical body area network devices in comparison to F-antennas," in *Recent Innovations in Sciences and Humanities*, Boca Raton, United States: CRC Press, 2025, pp. 302–306, doi: 10.1201/9781003606611-48.
[20] N. M. M. Dharani, T. Nikithaa, B. Rithika, and D. A. Joe, "Design of defected ground structure patch antenna for multiband applications," *2025 3rd International Conference on Advancements in Electrical, Electronics, Communication, Computing and Automation*, 2025, doi: 10.1109/ICAECA63854.2025.11012195.
[21] A. Chakraborty *et al.*, "A compact defected ground structure-based high isolated monopole MIMO antenna for USB band mobile satellite services," *International Journal of Communication Systems*, vol. 38, no. 10, 2025, doi: 10.1002/dac.70144.
[22] J. Xu and Y. Wang, "A defected ground structure design for reducing coupling in dual-band MIMO antennas," *Progress in Electromagnetics Research C*, vol. 158, pp. 93–101, 2025, doi: 10.2528/PIERC25061901.
[23] R. Kalaiyarasan, G. Nagarajan, and B. S. S. Kumar, "A dual-band sierpinski carpet fractal antenna with defected ground structure for wireless applications at ism band frequency (2.45 Ghz/5.8 Ghz)," *SSRN*, 2024, doi: 10.2139/ssrn.4691840.
[24] S. Pandav and S. K. Behera, "Design of koch fractal antenna with defected ground structure for s-band applications," *2023 IEEE Microwaves, Antennas, and Propagation Conference*, 2023, pp. 1-5, doi: 10.1109/MAPCON58678.2023.10463820.
[25] Z. Yu *et al.*, "A new koch and hexagonal fractal combined circular structure antenna for 4G/5G/WLAN applications," *Electronics*, vol. 14, no. 2, 2025, doi: 10.3390/electronics14020237.

BIOGRAPHIES OF AUTHORS

Raju Thommandru received B.Tech. degree in Electronics and Communication Engineering from Lakireddy Balireddy College of Engineering, Mylavaram, Andhra Pradesh, India, and M.Tech. degree in Digital Systems and Computer Electronics from Jayaprakash Narayan College of Engineering, Mahabubnagar, Telangana, India. He is currently pursuing Ph.D. degree, in Electronics and Communications Engineering at Saveetha School of Engineering, Thandalam, Chennai, India. He is in teaching profession for more than 17 years. He is currently working as associate professor in the Department of Electronics and Communication Engineering, Chalapathi Institute of Technology, Guntur. He has published 45 papers in national and international journals, conference and symposiums. He is a lifetime member of professional body like Indian Society for Technical Education (ISTE). His area of interest includes monopole and dipole antenna design, 5G communication, MIMO antenna, wireless communication, wireless sensor networks, RF, and microwave systems. He can be contacted at email: raazu.thommandru@gmail.com.

Dr. Rengaraj Saravanakumar completed his B.E. degree in Electronics and Communication Engineering in the year 2005 from Alagappa Chettiar Government College of Engineering and Technology, Karaikudi and subsequently he completed M.E. degree in Communication Systems at PSG college of Technology, Coimbatore. He completed his Ph.D. in the area of Antenna Design and Wireless Communication from Anna University, Chennai in the year 2019. He has 11 years of teaching experience. Currently he is working as assistant professor in the Department of Electronics and Communication Engineering, Hindusthan Institute of Technology, Coimbatore from 2009. His area of interest includes monopole and dipole antenna design, micro strip resonator, wireless communication, wireless sensor networks, RF, and microwave systems. His patent was graded by the IP Australian Government and one more patent published in Indian Patent. He has published 10 international journal papers and 20 international/national conference papers. In addition, he has published one book, in the title of electromagnetic fields. He is a reviewer of AdHoc and sensor wireless networks. He is a lifetime member of various professional bodies like ISTE and IEI. He received funds from the Central Government and State Government, Science and Technology Departments. He can be contacted at email: drsaravanakumar.asrith@gmail.com.